Front. Earth Sci. 2024, 18(3): 623−636
https://doi.org/10.1007/s11707-024-1103-4

RESEARCH ARTICLE

# Gas content evaluation in deep coal seam with an improved method and its geological controls

**Haiqi LI[1,2,3], Shida CHEN (✉)[1,2,3], Dazhen TANG[1,2,3], Shuling TANG[1,2,3], Jiaosheng YANG[4]**

1 School of Energy Resource, China University of Geosciences (Beijing), Beijing 100083, China
2 Coal Reservoir Laboratory of National Engineering Research Center of Coalbed Methane Development and Utilization, Beijing 100083, China
3 Beijing Key Laboratory of Unconventional Natural Gas Geological Evaluation and Development Engineering, Beijing 100083, China
4 China Petroleum Exploration and Development Research Institute, Langfang 065000, China



**Abstract** An improved evaluation method for estimating gas content during the inversion process of deep-burial coal was established based on the on-site natural desorption curves. The accuracy of the US Bureau of Mines (USBM), Polynomial fitting, Amoco, and the improved evaluation methods in the predicting of lost gas volume in deep seams in the Mabidong Block of the Qinshui Basin were then compared. Furthermore, the calculation errors of these different methods in simulating lost gas content based on coring time were compared. A newly established nonlinear equation was developed to estimate the minimum error value, by controlling the lost time within 16 min, the related errors can be reduced. The improved evaluation was shown to accurately and rapidly predict the gas content in deep seams. The results show that the deep coal bed methane accumulation is influenced by various factors, including geological structure, hydrodynamic conditions, roof lithology, and coalification. Reverse faults and weak groundwater runoff can hinder the escape of methane, and these factors should be considered in the future exploration and development of coalbed methane.

**Keywords** deep coalbed methane, Mabidong Block, lost gas, geological controls

## 1 Introduction

As a type of clean natural gas resource, coalbed methane (CBM) has gained significance as a vital component of the natural gas supply in countries such as China, the US, Australia, Canada, and others (Golding et al., 2013; Bustin and Bustin, 2016; Qin et al., 2018; Connell et al., 2019). In China, exploration results demonstrate that deep coal reservoirs possess abundant recoverable CBM resources, with estimated reserves of 22.5 × $10^{12}$ $cm^3/g$ occurring at depths of 1000−2000 m (Fu et al., 2009; Luo et al., 2017; Ou et al., 2018). These reserves account for 61.2% of CBM resources below a depth of 2000 m (Luo et al., 2017). Gas content is a key parameter for resource reserve evaluation, sweet spot selection, and production technology determination. Hence, achieving an accurate assessment of gas content holds great significance in CBM development (Xu et al., 2020; Jing et al., 2021; Miao et al., 2022).

Chronologically, determining the gas content is essential for both safety considerations and preventing coal and gas outbreaks (Kissell et al., 1973; Diamond and Schatzel, 1998; Wang et al., 2015). The commercial development of CBM has spurred advancements in gas content measurement technology (Liu and Harpalani, 2013). Currently, gas content testing methods are divided into indirect and direct methods. The indirect method (isothermal adsorption test) measures gas content by varying gas pressure under known reservoir pressure and temperature conditions (Metcalfe et al., 1991; Saghafi, 2017). Howere, there is a strong assumption of temperature limit and single gas saturation which is inconsistent with *in situ* conditions, and therefore, the indirect method is more applicable for assessing the maximum gas content (Hou et al., 2020; Lei et al., 2023). For the direct method, the gas lost during drilling is the lost gas, the gas measured in the desorption tank is the desorption gas, and the gas remaining in the desorbed sample is the residual gas. The total content is the sum of the lost gas, desorbed gas, and residual gas. Various methods are used in engineering applications to estimate lost gas, including the US Bureau of Mines (USBM)

Received March 26, 2023; accepted July 21, 2023

E-mail: cugb_csd@126.com

method, polynomial fitting method, and Amoco curve fitting method (Bertard et al., 1970; Kissell et al., 1973; Smith and Williams, 1984; Diamond and Schatzel, 1998; Shtepani et al., 2010; Deng et al., 2023). However, discrepancies in overall gas content calculations arise due to the identification of the time zero point and the selection of the desorption data segment used to infer the amount of lost gas.

The direct method is founded on Fick's diffusion law, where the gas diffusion model of uniform coal particles serves as the solution for gas content projection. Although estimating lost gas and residual gas, based on field measurements of desorption curves of coal cores, has improved the accuracy of measuring coal seam gas content, certain challenges remain. The nature of the desorption curve segments used to estimate total gas content is the difference in desorption time. Long or short desorption times for estimating total gas content can result in large errors in the calculation of the curves, leading to a discrepancy between the total gas content and the actual. Therefore, it is essential to carefully consider the desorption time to ensure accurate measurement of the desorbed gas and improve the estimation of the total gas content.

In addition, the geological characteristics of the reservoir, such as depositional system, coal distribution, tectonic setting, coal rank, gas generation, and fluid dynamics must be considered when assessing the gas content (Scott, 2002; Wang et al., 2023). Coal rank and reservoir pressure have positive effects on gas content, and the increase in deep temperature is not conducive to the occurrence of gas. Strong runoff recharge areas tend to carry away methane and disrupt gas accumulation, while weak runoff recharge areas are more conducive to gas accumulation (Cai et al., 2014; Li et al., 2018a; Wang et al., 2018a). Faults significantly impact the abundance of CBM resources and favorable areas (Kinnon et al., 2010; Hemmings-Sykes, 2012; Chen et al., 2020; Yang et al., 2023). The CBM exploration strategies ignore geological factors, which will decrease production capacity. Thus, evaluating gas content based on stratum and selecting favorable areas, considering reservoir geological characteristics comprehensively, serves as the foundation and focal point of deep CBM exploration.

The primary objective of this study is to investigate the gas-bearing characteristics of the Mabidong block. To improve the evaluation process for quickly estimating gas content, a novel approach based on the termination limit of natural desorption was proposed. A limit is established when the gas release is less than 1010 $cm^3/d$ for seven consecutive days. To ensure accuracy and minimize errors arising from variations in desorption data, gas content was rapidly calculated using complete desorption curves. By utilizing field data rather than relying on assumed ideal conditions, the quantified results can effectively guide the assessment of CBM resources and reserves.

## 2 Geological setting and method

### 2.1 Geological setting

The Qinshui Basin is a Mesozoic basin originating from the Late Paleozoic Craton Basin with a simple internal structure and abundant CBM resources. The entire basin is a bilaterally symmetric co-inclined basin surrounded by Wutai Mountain, Zhongtiao Mountain, Huo Mountain, and Taihang Mountain (Cai et al., 2011; Teng et al., 2015). The Mabidong block is located in the south-east Shanxi Province, spanning Linfen and Jincheng (Figs. 1(a) and 1(b)). The study block has experienced four tectonic movements in terms of structure. These movements are known as the Indosinian, Yanshanian, Early Himalayan, and Late Himalayan orogenies (Cai et al., 2011; Cao et al., 2020) . In the early stage of the Indosinian movement, the North China Platform began to activate and disintegrate, and a small number of east–west folds developed under the action of the north–south principal compressive stress; during the Yanshan movement, the strong orogenic movement made the Shanxi block continue to uplift. Meanwhile, the degree of coal metamorphism is influenced by the intrusion of stratigraphic magma (Cai et al., 2011); the conversion of principal compressive stresses during the early Himalayan orogeny and the late Himalayan orogeny led to the uplift and erosion of faults and strata (Teng et al., 2015; Wang et al., 2018b). The stratigraphic column and parameters of the coal-bearing strata in the study area are shown in Fig. 1(c).

### 2.2 Samples and methods

Samples of coal cores from 11 wells were collected and desorbed in situ to determine the desorbed gas content according to the Chinese Standard GB/T 19559-2008 for CBM content determination. The number of samples and testing items are shown in Table 1. All coring work used the same gas collection procedure, and the completion of the experimental procedures after routine coring was done by the China Petroleum Exploration and Development Research Institute. At the desorption temperature of the storage tank, the desorption tank with the sample seal is quickly placed in the thermostat and connected to the gas flow meter through a hose connecting the tank. During the test, the valve of the desorption tank was opened so that the desorbed gas in the tank will enter the flowmeter cylinder, the cylinder level was adjusted, the cylinder water level reading was recorded before and after desorption, the desorption valve was closed, and the desorbed gas content was calculated (Fig. 2).

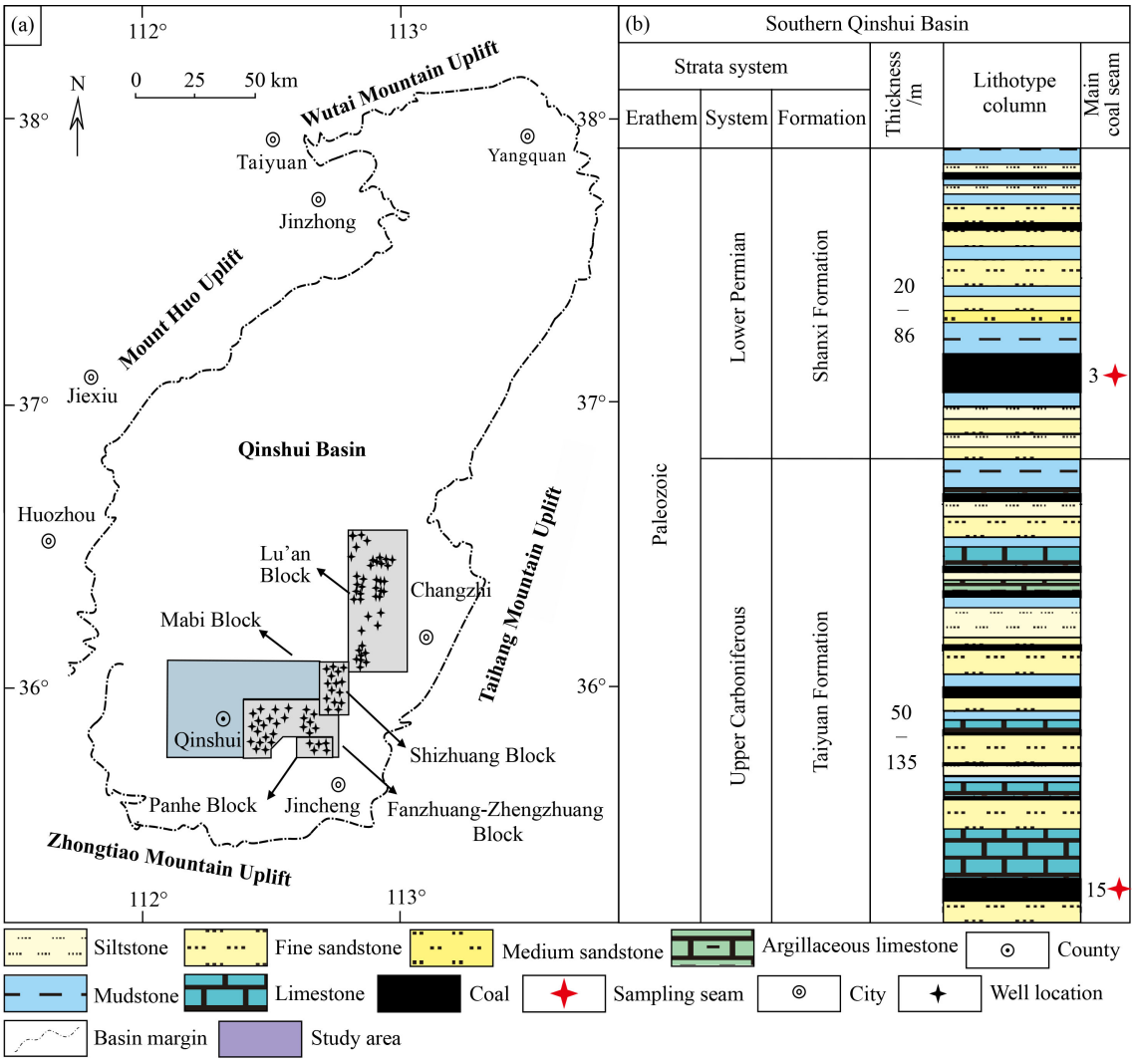


**Fig. 1** Geological background of the Qinshui Basin (modified from (Cai et al., 2014)). (a) Location of the basin. (b) Location of the Mabidong study area. (c) Composite stratigraphic columns in the Mabidong block.

**Table 1** Sample collection and testing information table

| Well Name | Number of samples collected | | Number of gas content test samples | Industrial analysis and determination sample number |
|---|---|---|---|---|
| | 3# | 15# | | |
| 6 | 6 | 7 | 12 | 6-3-1, 6-15-1 |
| 16X | 1 | 2 | 3 | 16X-3-1, 16X-15-1 |
| 27 | 6 | 4 | 10 | 27-3-1, 27-15-1 |
| 57 | 5 | 4 | 9 | 57-3-1, 57-15-1 |
| 58 | 7 | 4 | 11 | 58-3-1, 58-15-1 |
| 59 | 6 | 2 | 8 | 59-3-1, 59-15-1 |
| 66 | 5 | 5 | 10 | 66-3-1, 66-15-1 |
| 67 | 5 | 4 | 9 | 67-3-1, 67-15-1 |
| 69 | 4 | 3 | 7 | 69-3-1, 69-15-1 |
| 72 | 5 | 3 | 8 | 72-3-1, 72-15-1 |
| 2 | 7 | 3 | 10 | 2-3-1, 2-15-1 |

Notes: 6-3-1 refers to the sample 1 of the 3 # coal seam in the 6 well names, other sample numbers are similar.

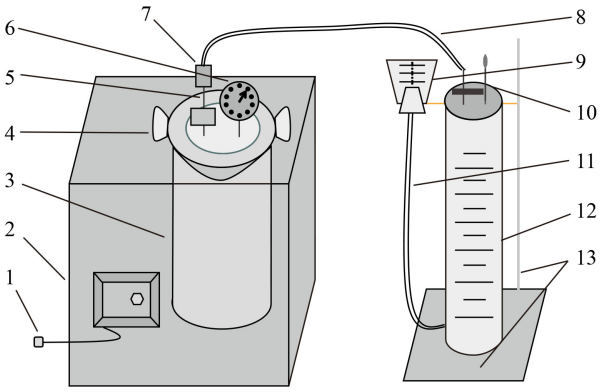


**Fig. 2** Natural desorption device (AQSIQ , 2008): 1. thermostat power supply, 2. thermostatic device, 3. desorption tank, 4. tank cover, 5. air valve, 6. pressure gauge, 7. quick connector, 8. exhaust pipe, 9. conical bottle, 10. air valve, 11. drain pipe. 12. measuring cylinder, 13. meter bases and stands.

## 3 Results

### 3.1 Different methods to determine gas content

#### 3.1.1 USBM direct method

Bertard was the first to propose a direct method for testing the CBM content (Bertard et al., 1970), which was further developed by the US Bureau of Mines (Kissell et al., 1973). The USBM approach employs a model that assumes a "single pore" through which diffusion occurs, and where a constant surface concentration of 0 $cm^3/g$ serves as the boundary condition. This method is founded on the principle that diffusion behavior can be characterized by this single pore, allowing for a simplified analysis of the process. It is given by (Mavor et al., 1990):

$$V_{Da} = 1 - \frac{6}{\pi^2}\sum_{n=1}^{\infty}\frac{\exp\left(-n^2\pi^2 T\frac{D}{r^2}\right)}{n^2}, \tag{1}$$

where the dimensionless gas concentration is $V_{Da}$, and the diffusion time, diffusion coefficient, and particle radius are denoted by $T$ (min), $D$ ($cm^2$/min), and $r$ (cm), respectively.

Bertard et al. (1970), and Smith and Williams (1984) suggested using the first 20% and 50% of the desorbed gas to assess the lost gas, respectively. In addition, the difference in drilling fluid media, the time when drilling encounters the coal seam and the time when the coring barrel is lifted halfway up the wellbore can be used as time zeros. The variation in lost time results in differences in lost gas content. (Fig. 3, Table 2). When the time of encountering the coal seam is used as the time zero, part of the lost gas is relatively low (Fig. 3(a)), which is negligible compared with the desorbed gas. For certain samples (as shown in Fig. 3(f)), the time when the coring is lifted to half of the wellbore as the time zero, and using the first 50% of the desorbed gas as the basis for lost gas calculation yields a relatively high percentage of lost gas, comprising 35.52% of the total desorbed gas. Hou et al. (2020) employed a method that utilized only half of the natural desorption data to determine lost gas from deep coal samples. In some cases, this resulted in a slight or negative lost gas measurement, indicating that the method may not be universally applicable.

In accordance with the national standard GB/T19559-2008, the USBM direct method linear section extrapolation allows for the calculation of lost gas volume. This calculation is performed by considering half the time of core extraction lift to the wellbore as time zero and using the first 20% of desorbed gas as the reference point. In engineering applications, water is commonly employed as the drilling fluid medium. Upon reaching the halfway point to the drilling depth, the pressure in the reservoir and drilling fluid is equalized, making it a logical time zero for analysis.

#### 3.1.2 Polynomial fitting and the Amoco method

Calculation of lost gas can be achieved by a number of methods, including the direct method of polynomial fitting (Lin et al., 2023; Zhao et al., 2023). The polynomial fitting method involves the following expression:

$$V_d = a\sqrt{T}^2 + b\sqrt{T} - c, \tag{2}$$

$$V_d = a\sqrt{T}^3 + \sqrt{T}^2 + c\sqrt{T} - d, \tag{3}$$

where $a$, $b$, $c$, and $d$ are curve-fitting parameters. Similarly, the constant term is the amount of lost gas.

Waechter et al. (2004) fitted all available desorption data creating the fitting method known as the "Amoco method". Again, based on the assumption of a "unipore" model and keeping just the first term of the equation, the following relationship is obtained:

$$v_d' = (V_l + V_d)\left[1 - \frac{6}{\pi^2}\exp\left(\frac{-D\pi^2 T}{r^2}\right)\right] - V_l, \tag{4}$$

where, $v_d'$ is the amount of desorbed gas corresponding to desorption time $t$, $cm^3/g$; lost gas can be obtained by curve fitting the data.

Here, different direct methods are used to calculate lost gas. Different desorption data are selected for polynomial fitting to obtain a downward convex curve, and the value corresponding to the time zero of the curve time is the lost gas. In this study, polynomial fits were obtained by selecting data points at different times in the early stages of desorption. Figure 4(a) shows that fewer data points are selected. The larger the intersection of the curve with the $Y$-axis, the less gas is lost. If the full desorption data are selected to fit, the lost gas loses the meaning of the

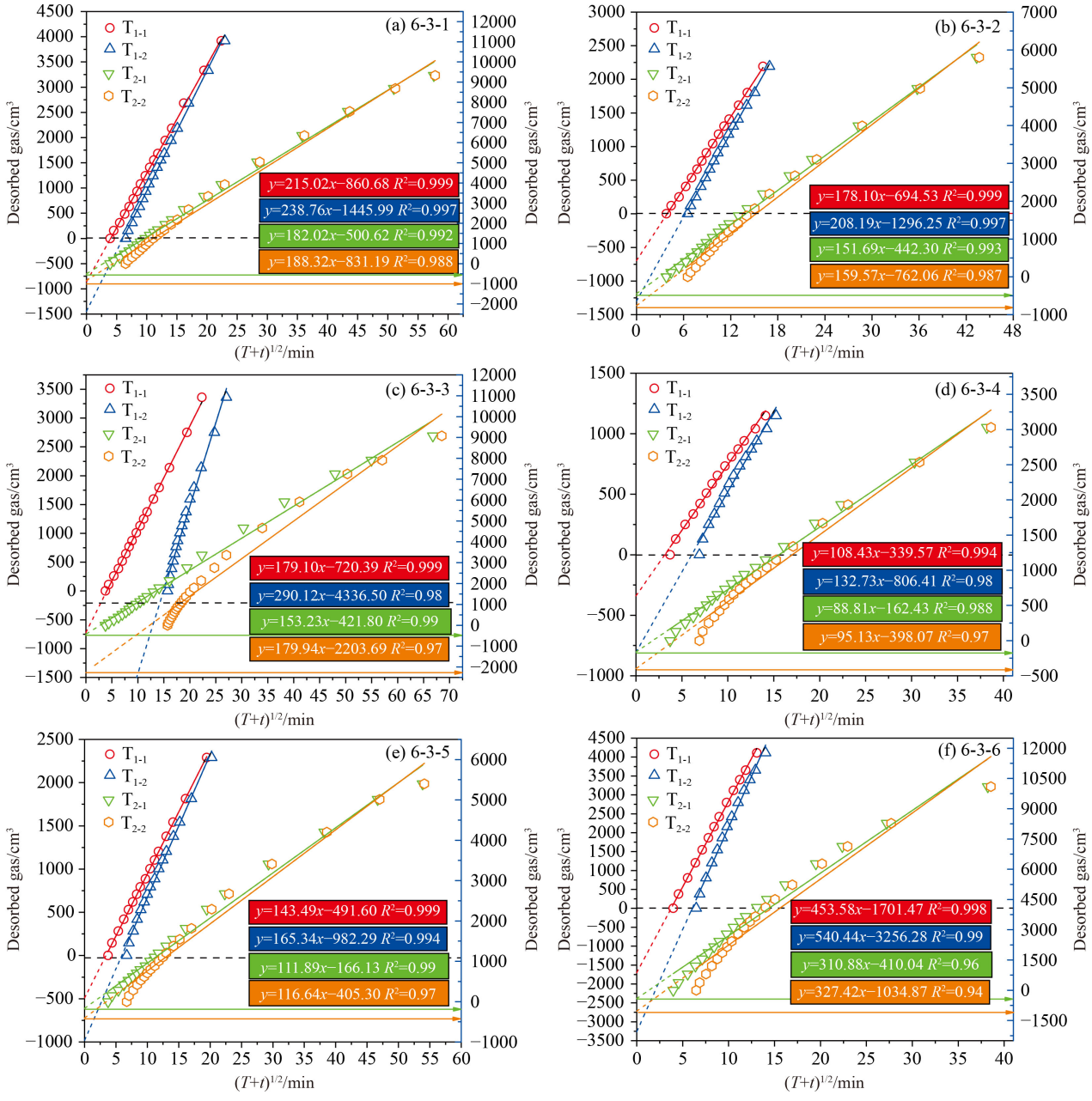


**Fig. 3** Lost gas estimation at different time zeros.

**Table 2** Estimation of lost gas content under different calculation standards

| Calculation standard | Lost gas content/cm³ | | | | | |
|---|---|---|---|---|---|---|
| | 6-3-1 | 6-3-2 | 6-3-3 | 6-3-4 | 6-3-5 | 6-3-6 |
| $T_{1-1}$ | 860.68 | 694.53 | 720.39 | 339.57 | 491.6 | 1701.47 |
| $T_{1-2}$ | 1445.99 | 1296.25 | 4336.5 | 806.41 | 982.29 | 3256.28 |
| $T_{2-1}$ | 500.62 | 442.3 | 421.8 | 162.43 | 166.13 | 410.04 |
| $T_{2-2}$ | 831.19 | 762.06 | 2203.69 | 398.07 | 405.3 | 1034.87 |

Notes: $T_{1-1}$ refers to the time when the coring is lifted to half of the wellbore as the time zero and the first 20% of the desorbed gas is used as the calculation standard for the lost gas; $T_{1-2}$ refers to the first 50% of the desorbed gas is used as the calculation standard for the lost gas; $T_{2-1}$ refers to the time when drilling encounters the coal seam as the time zero and the first 20% of the desorbed gas is used as the calculation standard for the lost gas; $T_{2-2}$ refers to the e first 50% of the desorbed gas is used as the calculation standard for the lost gas.

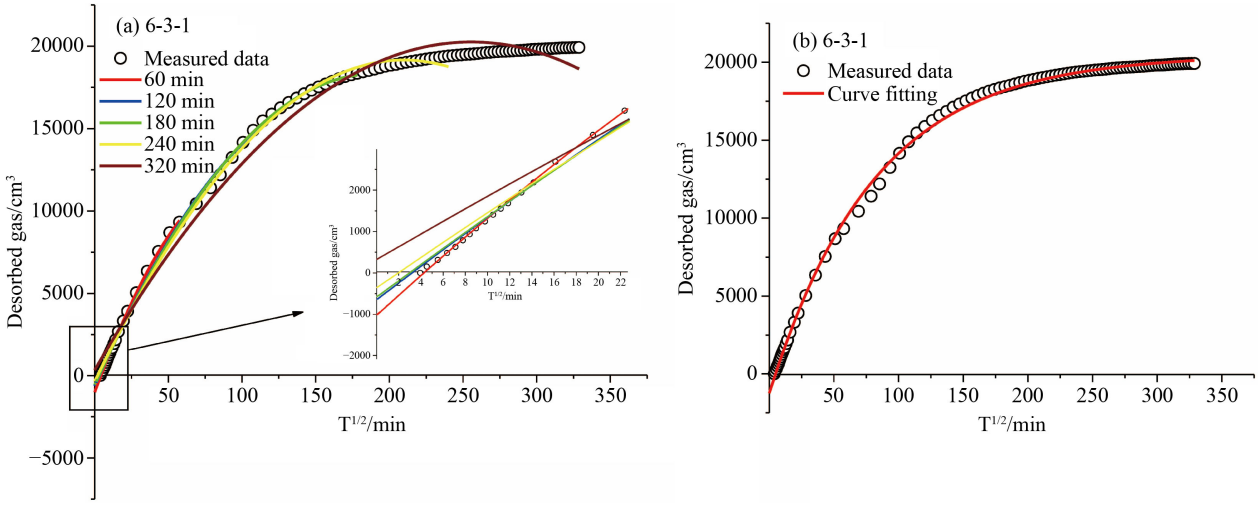


**Fig. 4** Calculation of lost gas content by (a) polynomial fitting method, (b) Amoco method.

equation. According to the data points of 60 min, 120 min, 180 min, and 240 min, the fitted lost gas content is 1029.24 $cm^3$, 651.64 $cm^3$, 586.85 $cm^3$, and 364.78 $cm^3$, respectively. The maximum lost gas content obtained by the Amoco method was 1281.73 $cm^3$ (Fig. 4(b)).

### 3.2 Improved evaluation

The improved evaluation method is based on the second law of Fick's diffusion, which assumes uniform gas diffusion at time zero and the total gas content is the solution of the geometric shape of a spherical coal sample with zero boundary conditions (Zhao et al., 2019; Li et al., 2022). The desorption gas was obtained through on-site testing, while the residual gas was obtained through laboratory testing. Utilizing the on-site desorption outcomes, estimates can be made for the loss gas and total gas content. By analyzing the natural desorption data of multiple samples from 11 wells in the field, the following equations were established:

$$v'_{\mathrm{d}} = a \times \exp\left(\frac{-\sqrt{T+t}}{b}\right) + c, \tag{5}$$

where $v'_{\mathrm{d}}$ is cumulative desorption content ($cm^3$); the total amount of gas comprising both the maximum desorbed gas and the residual gas can be denoted by the symbol $c$ ($cm^3$). The total gas content is denoted by $a$ ($cm^3$); $b$ is the dimensionless time determined by desorption time, diffusion coefficient, and particle radius.

The core sample is desorbed from time zero, then the desorbed gas will be

$$v'_{\mathrm{d}} = V_{\mathrm{l}} + V_{\mathrm{d}}. \tag{6}$$

So, the following relationship exists between the lost gas and the residual gas:

$$V_{\mathrm{l}} = v'_{\mathrm{d}} - V_{\mathrm{d}}, \tag{7}$$

$$V_{\mathrm{r}} = V - V_{\mathrm{l}} - V_{\mathrm{d}}. \tag{8}$$

For instance, the natural desorption full data of the 6-3-1 sample was subjected to fitting using Eq. (7), and the resulting curve is presented in Fig. 5. The point where the extended curve intersects the ordinate corresponds to the lost gas, while the constant term represents the total gas content. The lost gas calculation for this sample yielded a value of 1281.73 $cm^3$, the highest among all samples tested. Additionally, the calculated total gas content volume using this method was 21763.47 $cm^3$, which exceeded the value obtained through the USBM direct method (20862.99 $cm^3$).

### 3.3 Methane adsorption isothermal method

Isothermal adsorption tests allow for obtaining the relationship between methane adsorption and pressure at reservoir temperature (Yang and Liu, 2019).

$$V = \frac{V_L P}{P + P_L}. \tag{9}$$

The adsorbed gas content ($V$) is expressed in units of

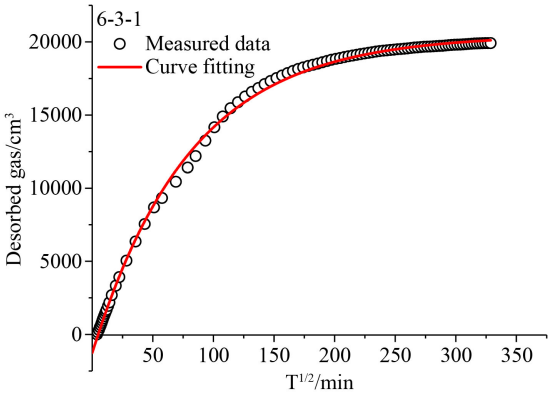


**Fig. 5** Gas content evaluation by the improved evaluation.

$cm^3/g$ and is influenced by the Langmuir volume ($V_L$), also measured in $cm^3/g$. Gas pressure ($P$) is measured in MPa, while Langmuir pressure ($P_L$) is also expressed in units of MPa.

Figure 6 shows the theoretical adsorption capacity of methane at variable gas pressure, the adsorption capacity increases with increasing gas pressure. The test sample had a Langmuir pressure of 2.18 MPa and a Langmuir volume of 33.04 $cm^3/g$. The test sample 6-3-1 has a gas content of 28.99 $cm^3/g$ at a pressure of about 15.6 MPa, assuming that the methane gas is saturated. Notably, the coal seam is saturated by default in the isothermal adsorption test. This strong assumption of single gas saturation makes the gas content obtained by the test higher than the direct method test results, which deviates from the actual situation.

## 4 Discussion

### 4.1 Gas content evaluation and comparison

#### 4.1.1 Simulation and accuracy of estimating gas content

The lost gas content was simulated and estimated by refining the lost time during coring and compare the calculation accuracy of different methods (Xu et al., 2020). According to the actual coring process, lost gas time is divided into core lost time $t_1$ and surface exposure time $t_2$.

Assuming that the time from the start of coring to reach the ground, $t_s$ can be expressed as

$$t_s = t_1 + 2t_3. \tag{10}$$

where $t_3$ is the time of desorption in the desorption tank, then get the simulated lost gas time:

$$t'_s = \frac{1}{2}t_s + t_2, \tag{11}$$

establish the relationship between $t_s$ and $t'_s$:

$$t_s = t'_s + t_3. \tag{12}$$

Therefore, the following relationship exists between the gas content corresponding to the corresponding time:

$$V_s = V'_s + V_{t_3}, \tag{13}$$

where $V_s$ is the lost gas assumed to correspond at the time $t_s$; $V'_s$ is the lost gas assumed to correspond at the time $t_3$.

Under varying simulation time conditions, the lost gas content is estimated according to Eqs. (10) and (13). The simulated and estimated times will coincide provided that the sum of the time taken for lifting the core to the wellbore and the duration it remains enclosed in the desorption tank equals the simulated time at which the sample arrives at the surface. In this situation, $V_s(t_s = 8) = V'_s(t'_s = 8)$, the 8 min time is determined according to the actual drilling sampling time on site. For a simulated lost gas time of 28 min, the assumed sample desorption time is 10 min.

The gas content data measured in the field show an exponential relationship between gas desorption rate and desorption time (Fig. 7). Sampling depth increased from 1128.16 m (6-3-1) to 1390.07 m (16X-3-1), and initial desorption rate increased from 31.07 $cm^3/min$ to 103.35 $cm^3/min$, where the desorption rate of the 58-3-1 sample was 63.62 $cm^3/min$. The determination of lost time is crucial for accurately estimating the lost gas content, particularly during the initial phase of desorption, as it has a pronounced effect on the desorption rate.

The improved evaluation results were utilized to perform a curve fit on the measured data from the samples, as illustrated in Fig. 8. For lost gas times of 28 min, 48 min, and 68 min, the estimated lost gas value is 1437.06 $cm^3$, 1592.3 $cm^3$, and 1764.99 $cm^3$, respectively. The rate of desorption decreases when the

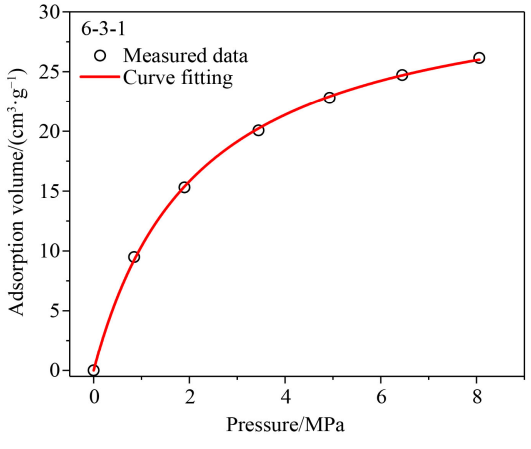


**Fig. 6** 6-3-1 Sample isothermal adsorption test.

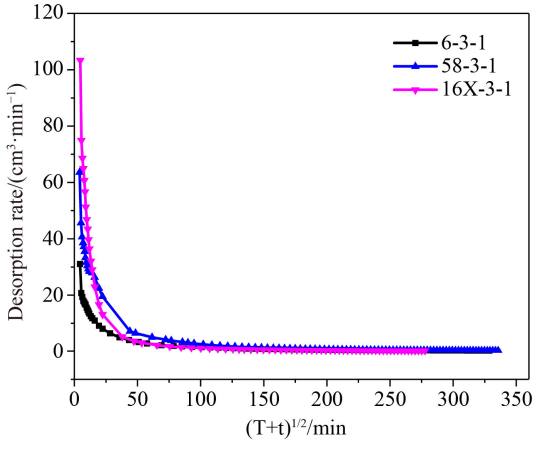


**Fig. 7** Relationship between desorption rate and the square root of desorption time for coal samples with different buried depths.

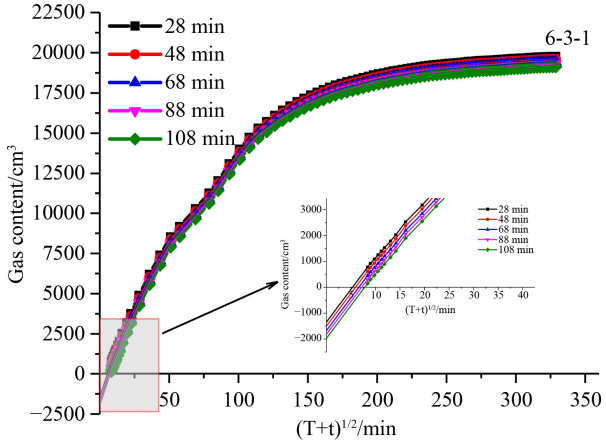


**Fig. 8** Extrapolation calculation of lost gas for simulating different lost time.

simulated lost gas times reach 88 min and 108 min. Additionally, the increase in extrapolated lost gas values slows down with an increasing trend. During the simulation, the estimated lost gas amounts closely approximate 1911.69 $cm^3$ and 2067.02 $cm^3$ at the simulated lost gas times of 88 min and 108 min, respectively.

The error value is defined by the estimated amount of gas lost and the actual amount of gas lost, expressed as $(V_s - V_s')/V_s' \times 100\%$. The error is plotted based on the method discussed above to evaluate the lost gas (Fig. 9). For the same fitting method, the lost gas time leads to differences in error values. The maximum error values of 76.30%, 69.61%, and 61.27% were obtained for the Polynomial, Amoco, and improved evaluations, respectively, all of which exceeded 50%. Among all fitting methods, the error value calculated by the improved evaluation is the smallest. In practical engineering applications, the core lifting time usually does not exceed 2 min per 100 m of well depth. In this study, samples were sealed within 10 min of reaching the surface and the maximum lost gas time (24.5 min) was less than the simulation time (28 min). Considering that the deep core taking time is relatively long, the calculation error can be further reduced by controlling lost time within 16 min, calculated as 15 min per 1000 m of core taking time and 1 min for sample loading time.

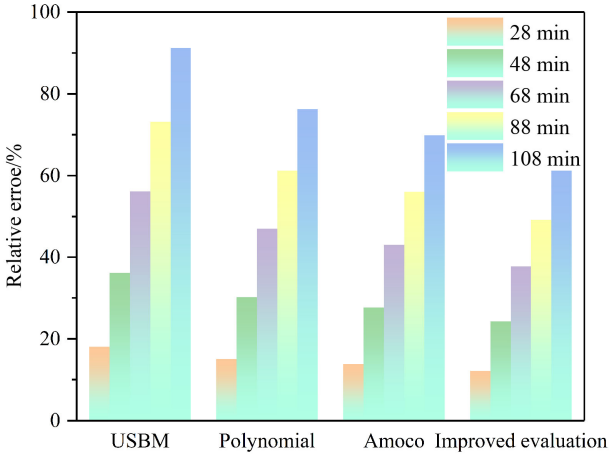


**Fig. 9** Lost gas error of different curve fitting methods.

### 4.1.2 Gas content evaluation and comparison

Desorption data collected and measured under controlled conditions are highly reliable. In practice, a thermostat is used to simulate the reservoir temperature for desorption measurements to avoid errors in total gas content due to desorption measurement limitations. The on-site desorption time exceeded 10000 min, with the resulting residual gas test revealing less than 2.35% of the total gas content. Consequently, the impact of residual gas can be deemed insignificant. Therefore, as emphasized in previous studies, an accurate estimation of lost gas is essential for an accurate assessment of total gas content (Li et al., 2018b; Dang et al., 2018).

While the USBM method is commonly used to determine the in situ content of CBM, its accuracy is still under investigation. Researchers have tested the CBM content through different methods (indirect method, laboratory simulation method), and a comparative study found that the USBM direct method may underestimate the gas content (Waechter et al., 2004; Dang et al., 2018). The Polynomial fitting method involves selecting different data segments to obtain fitted curves with distinct orthogonal points on the *y*-axis. Extending the range of data leads to differences and anomalies in the estimated lost gas (Fig. 4(a), Fig. 10). In contrast, the Amoco method and the improved evaluation method demonstrated only minimal differences in lost gas values. The Amoco method and the improved evaluation calculated 1.31 and 1.49 times more lost gas than those calculated by the USBM method, respectively.

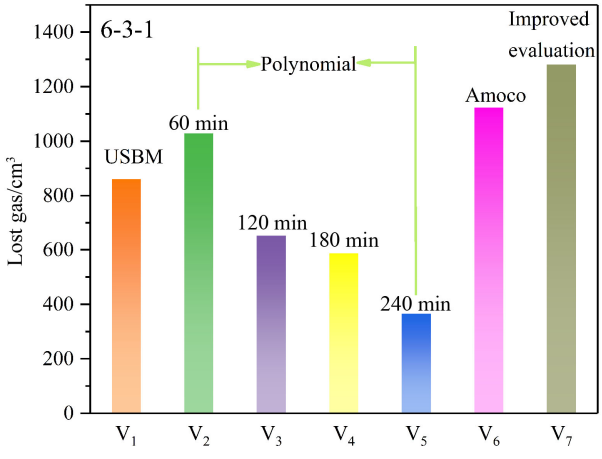


**Fig. 10** Comparison of lost gas content calculated using different methods.

Figure 11 depicts the results of the total gas content calculation using different methods. The USBM method, polynomial fitting method (selecting the first 60 min desorption data), and Amoco method calculated the gas content of the coal seam as 22.53 $cm^3/g$, 22.54 $cm^3/g$, and 22.69 $cm^3/g$, respectively. The total gas content obtained by the improved assessment is 3.5% higher compared to the national recommended standard calculation method. The in situ gas content of coal seams with different burial depths calculated with the national standard recommended method varies from 12.77 $cm^3/g$ to 20.64 $cm^3/g$. However, with the improved evaluation method, the in situ gas content obtained varies from 12.82 $cm^3/g$ to 28.87 $cm^3/g$. The total gas content obtained by the improved evaluation method is 4.22% higher than the total gas content value obtained by the recommended method of the national standard. This finding suggests that the cumulative gas production of some single wells is larger than the measured CBM resources.

#### 4.1.3 Implications for improving coring technology and gas content calculation

As exploration activities for CBM resources increase, methods to accurately assess gas content have received extensive attention. The USBM method serves as a widely adopted national standard recommended method to evaluate in situ gas content. It relies on two crucial parameters: drilling fluid density and reservoir temperature. The choice of data for the straight line segment of the desorption curve is a major source of error in estimating the lost gas. For this study, the range of data segments used to evaluate the amount of lost gas was determined.

The improved evaluation proposed in this paper can quickly evaluate the gas content of each component, which is significantly better than other direct methods in terms of accuracy. Yet, the gas content is obtained based on natural desorption data *in situ*. The accuracy of the calculation can be improved by using the pressure-preserving coring method as well as simulating the natural desorption in the *in situ* condition state. To further verify the accuracy of the improved evaluation, adhering to high standards and requirements for coring, gas collection, and testing is crucial.

### 4.2 Factors controlling gas content distribution

#### 4.2.1 Coalification and coal quality

The evolution of pores is directly influenced by the process of coalification, which consequently leads to an expansion in the volume of micropores and gas content (Gentzis et al., 2006). Thus, coalification is considered a critical factor in controlling gas content. Figure 12 visually illustrates the relationship between gas content and coal rank, providing a clear representation of their correlation. Generally, gas content and coal rank are positively correlated, which can be attributed to the increase in adsorption capacity resulting from increased coalification (Gentzis et al., 2006).

Extensive studies have shown that coal characteristics, including moisture, ash, volatile matter, and calorific value, play significant roles in determining the total gas content of coal seams (Butland and Moore, 2008; Warwick et al., 2008; Dai et al., 2023). However, there is no clear correlation between coal quality and gas content in the coal seam, as illustrated in Figs. 13(a)−13(d). It is possible that other geological factors are responsible for the variations in CBM reservoir content in the Mabidong Block.

#### 4.2.2 Burial depth and coal thickness

Burial depth is known to control coalification and positively affect gas generation and preservation, as previously

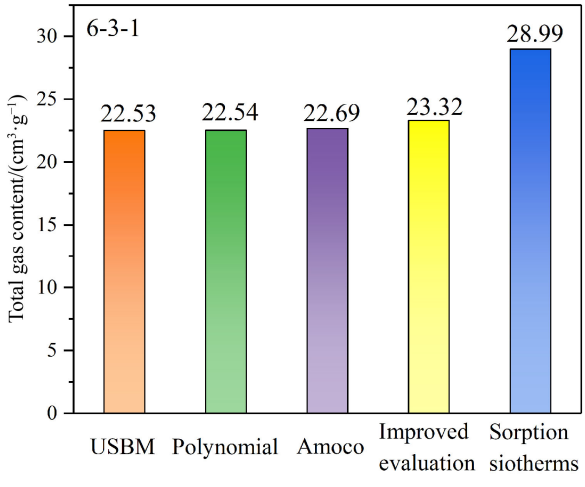


**Fig. 11** Total gas content by different estimation methods.

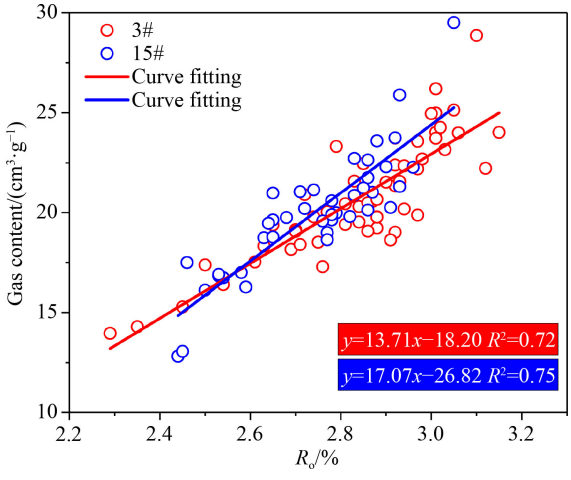


**Fig. 12** Correlation between $R_{o,\,max}$ and gas content.

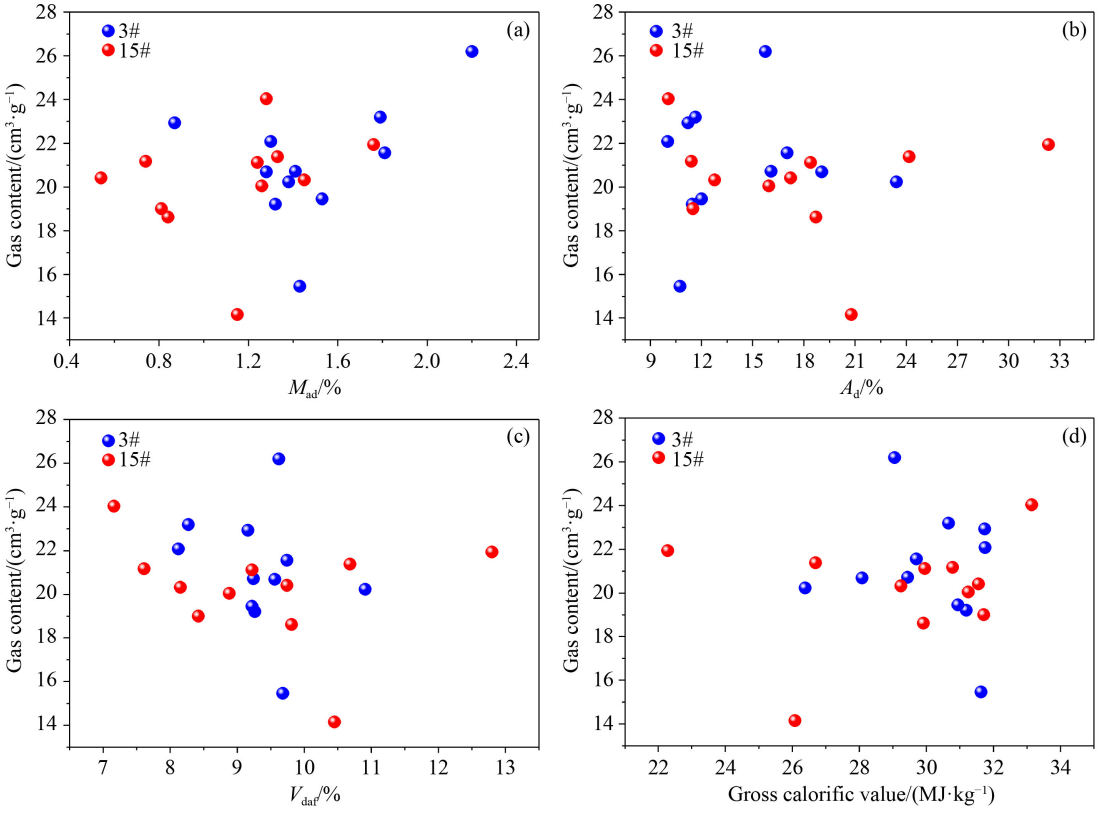


**Fig. 13** Effect of (a) moisture, (b) ash yield, (c) volatile matter, and (d) gross calorific to the gas content.

noted by Chen et al. (2021). However, the relationship between the gas content of the 3# coal seam/15# coal seam and the burial depth (Fig. 14(a)) shows no obvious correlation. While depth of burial weakly controls the CBM content in the study area, the CBM content of different logging wells exhibits an overall upward trend with increasing depth, particularly beyond 1400 m. This phenomenon can be attributed to the higher in situ reservoir pressure of the 15# coal seam (9.61 MPa) compared to that of the 3# coal seam (8.6 MPa), providing an explanation for the observed trend.

Coal seams have a dual role as both source rocks and reservoir rocks. Deep CBM reservoirs are more favorable for the adsorption of gas molecules as they have highly developed micropores, compared to shallow CBM reservoirs. Ideally, the thick coal seam provides a large reservoir space that enhances the CBM content. However, Fig. 14(b) illustrates the absence of a correlation between the gas content of the coal seam and its thickness. This can be explained by simple geological formations that result in slight variations in coal seam thickness and depositional environment.

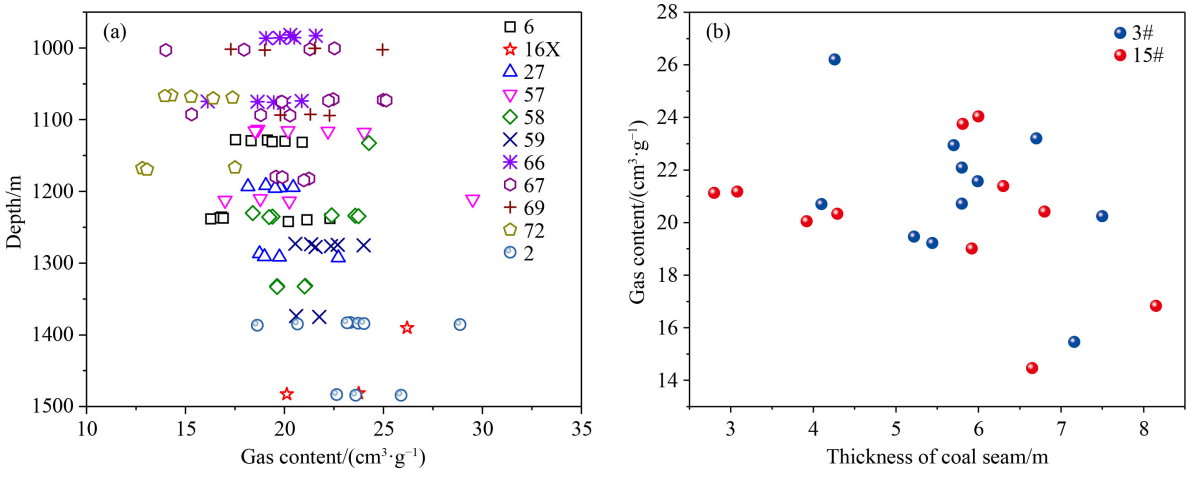


**Fig. 14** Relationship of (a) burial depth and (b) coal thickness with gas content.

#### 4.2.3 Hydrodynamic conditions

Hydrodynamic conditions are critical conditions affecting CBM reservoir formation (Gentzis et al., 2006; Chen et al., 2021). A substantial groundwater pressure facilitates the development of hydraulic plugging and sealing, which promotes the enrichment of CBM. When the groundwater runoff is strong, it intensifies the dissolution and escape of coal seams, resulting in lower gas content within the coal seams.

The hydrogeological unit of the study block includes four spring areas: Guangsheng Temple Spring in the north-west, Xin'an Spring in the north-east, Taipei Spring in the south-east, and Yanhe Spring in the south (Fig. 15). The Mabidong block is situated within a hydrodynamic stagnation area characterized by weak runoff, creating favorable hydrodynamic conditions for CBM enrichment. The 3# coal roof is weak water-bearing sandstone, and the bottom is a thick mudstone water-repellent layer, which has limited influence on gas content. Additionally, there exists a significant mudstone interlayer between the 15# coal and the upper limestone aquifer, which does not noticeably impact the gas content.

#### 4.2.4 Sealing conditions and tectonic controls

Changes in roof lithology and thickness cut off the connection between the aquifer and coal seam vertically, and at the same time have a protective effect on gas migration (Jin et al., 2015; Fu et al., 2016). When the roof is thin, the ability to suppress gas emission from coal seams will decrease. For instance, in Borehole 57 of Coal Seam 15# (Fig. 16(a)), the thickness of the limestone roof is 0.34 m, and the gas content is only 16.8 $cm^3/g$ (Fig. 16(b)); In Borehole 69 of Coal Seam 3#, the mudstone roof thickness is only 0.17 m, and the CBM content is 21.19 $cm^3/g$. Consequently, a thicker roof provides more favorable conditions for gas preservation.Geological structure plays a pivotal role in determining the distribution of coal seams and rock formations on both the roof and floor. This, in turn, indirectly impacts gas accumulation and migration, making it a crucial factor in CBM enrichment (Bertard et al., 1970). The syncline is favorable for the occurrence of CBM, while the gas in the anticline may more easily to escape. Faults may destroy the sealing of roof rock layers and affect the gas storage capacity. Generally, normal faults provide channels for gas escape, and reverse faults form barriers to inhibit gas escape (Bertard et al., 1970; Kędzior et al., 2013; Zhu and Lin, 2015; Fu et al., 2016). Mabidong block is divided into three zones: the western slope belt, the central trough belt, and the eastern slope belt (Fig. 16(c)). The western slope belt has a simple structure, most of the faults are NNE-trending and local NE-trending, and the overall scale is small, with a fault distance of 15−30 m and an extension distance of 1.5−2.9 km. Comparatively, the central trough belt demonstrates greater complexity, characterized by well-developed NNE and NE trending

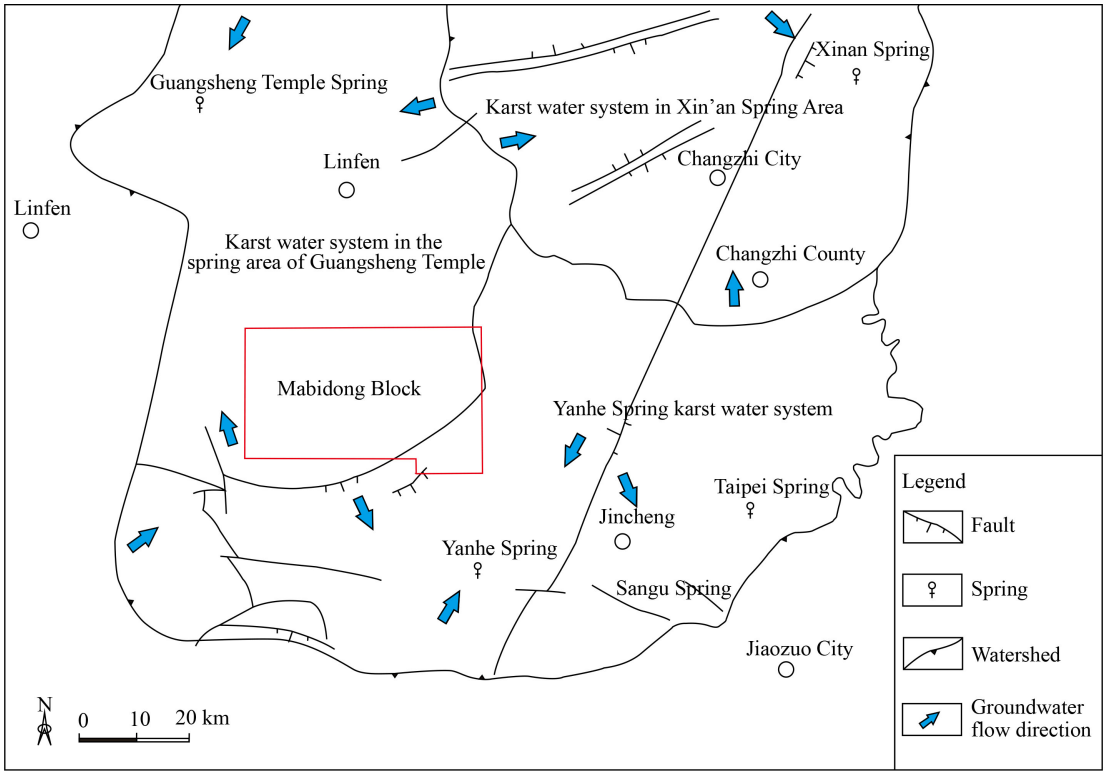


**Fig. 15** Groundwater dynamic zoning map in the study area.

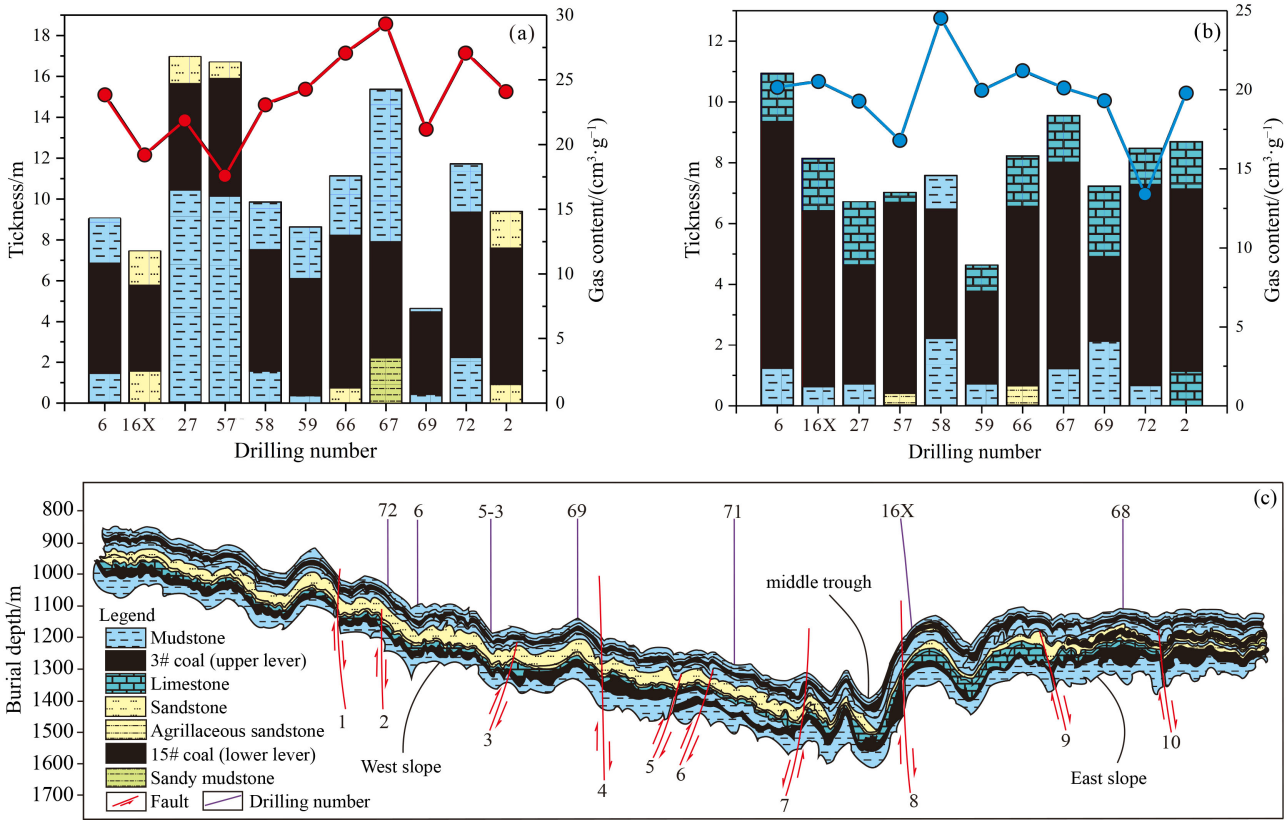


**Fig. 16** The control of lithology and tectonics on gas content in the study area. Relationship between roof and floor lithology and gas content: (a) 3#, (b) 15,. (c) Control of tectonics.

faults. On the other hand, the eastern slope belt displays a higher level of complexity, marked by a series of NNE-trending normal faults spaced 20–60 m apart, with extension distances ranging from 0.9 to 6.5 km. Although the structural characteristics of the eastern flank are more complex than those of the western flank, the strata in the eastern flank are generally gentler than those in the western flank.

The 3# and 15# coal seams within the block display distinct fault characteristics, with fewer faults observed in the west wing and a higher occurrence of developed faults in the east wing. Consequently, the west wing is more favorable for CBM preservation. The 3# coal seam shows more favorable conditions for CBM exploration than the 15# coal seam due to its less complex structural conditions. Based on the results of the fine tectonic interpretation, the northern part of the east flank is relatively stable with few faults, making it a key area for further deep CBM exploration.

## 5 Conclusions

In this study, we conducted extensive field investigations on the gas content of the 3# and 15# coal seams in the Mabidong block of the southern Qinshui Basin. The following are the main conclusions of our research.

1) Improved evaluation based on on-site natural desorption data enables quick estimation of total gas content. In addition, simulation analysis employing lost gas time indicates that the newly proposed nonlinear equation yields the smallest calculation error. Therefore, the improved evaluation is the most reliable for estimating the lost gas volume.

2) The distribution of CBM content in the Mabidong block is influenced by coal rank, roof lithology, hydrodynamics, and tectonic activity. The study area falls under the weak runoff area within the hydrodynamic stagnation zone, which is beneficial for CBM enrichment. In addition, the thick mudstone layer above and below the 3# coal seam acts as a water retention barrier, leading to gas retention and accumulation, making it a promising area for CBM exploration.

3) The Mabidong block is partitioned into the western slope belt, central trough belt, and eastern slope belt. The faults in the study area are predominantly NNE-trending with some local NE-trending faults, and they are relatively small in scale. Moreover, based on fine tectonic interpretation, both the west and east flanks demonstrate structural stability. Notably, the 3# coal seam within the block presents fewer faults, making it more favorable for CBM development. Conversely, the eastern slope belt emerges as a key region of interest for future deep CBM exploration.

**Acknowledgments** The authors thank the China Petroleum Exploration and Development Research Institute for facilitating the work. This work was supported by the National Natural Science Foundation of China (Grant No. 42130802), and PetroChina Company Limited "14th Five Year Plan" Science and Technology Major Project (No. 2021DJ2301).

**Competing interests** The authors declare that they have no competing interests.

## References

AQSIQ S A C (2008). Method of Determining Coalbed Gas Content: GB/T 19559–2008. Bejing: China Standard Press

Bertard C, Bruyet B, Gunther J (1970). Determination of desorbable gas concentration of coal (direct method). Int J Rock Mech Min Sci Geomech Abstr, 7(1): 43–65

Bustin A M M, Bustin R M (2016). Total gas-in-place, gas composition and reservoir properties of coal of the Mannville coal measures, Central Alberta. Int J Coal Geol, 153: 127–143

Butland C I, Moore T A (2008). Secondary biogenic coal seam gas reservoirs in New Zealand: a preliminary assessment of gas contents. Int J Coal Geol, 76(1−2): 151–165

Cai Y, Liu D, Yao Y, Li J, Qiu Y (2011). Geological controls on prediction of coalbed methane of No. 3 coal seam in Southern Qinshui Basin, north China. Int J Coal Geol, 88(2−3): 101–112

Cai Y, Liu D, Zhang K, Elsworth D, Yao Y, Tang D (2014). Preliminary evaluation of gas content of the No. 2 coal seam in the Yanchuannan area, southeast Ordos Basin, China. J Petrol Sci Eng, 122: 675–689

Cao L, Yao Y, Cui C, Sun Q (2020). Characteristics of in-situ stress and its controls on coalbed methane development in the southeastern Qinshui Basin, north China. Energy Geosci, 1(1−2): 69–80

Chen S, Tao S, Tian W, Tang D, Zhang B, Liu P (2021). Hydrogeological control on the accumulation and production of coalbed methane in the Anze Block, southern Qinshui Basin, China. J Petrol Sci Eng, 198: 108138

Chen X, Li L, Yuan Y, Li H (2020). Effect and mechanism of geological structures on coal seam gas occurrence in Changping minefield. Energy Sci Eng, 8(1): 104–115

Connell L D, Pan Z, Camilleri M (2019). The variation in produced gas composition from mixed gas coal seam reservoirs. Int J Coal Geol, 201: 62–75

Dai L, Lei H, Cheng X, Li R (2023). Prediction of coal seam gas content based on the correlation between gas basic parameters and coal quality indexes. Front Energy Res, 10: 1096539

Dang W, Zhang J C, Tang X, Wei X L, Li Z M, Wang C H, Chen Q, Liu C (2018). Investigation of gas content of organic-rich shale: a case study from Lower Permian shale in southern north China Basin, central China. Geosci Front, 9(2): 559–575

Deng Z, Wang H, Jiang Z, Tian F, Ding R, Hou S, Li W, Li Y, Zhu J, Li L, Wang X (2023). Interpretation method for lost gas in deep coalbed and its application. Processes (Basel), 11(1): 200

Diamond W P, Schatzel S J (1998). Measuring the gas content of coal: a review. Int J Coal Geol, 35(1−4): 311–331

Fu H, Tang D, Xu H, Xu T, Chen B, Hu P, Yin Z, Wu P, He G (2016). Geological characteristics and CBM exploration potential evaluation: a case study in the middle of the southern Junggar Basin, NW China. J Nat Gas Sci Eng, 30: 557–570

Fu X, Qin Y, Wang G G, Rudolph V (2009). Evaluation of gas content of coalbed methane reservoirs with the aid of geophysical logging technology. Fuel, 88(11): 2269–2277

Gentzis T, Schoderbek D, Pollock S (2006). Evaluating the coalbed methane potential of the Gething coals in NE British Columbia, Canada: an example from the Highhat area, Peace River coalfield. Int J Coal Geol, 68(3−4): 135–150

Golding S D, Boreham C J, Esterle J S (2013). Stable isotope geochemistry of coal bed and shale gas and related production waters: a review. Int J Coal Geol, 120: 24–40

Hemmings-Sykes S (2012). The Influence of Faulting on Hydrocarbon Migration in the Kupe Area, South Taranaki Basin, New Zealand. Dissertation for Master's Degree. Wellington: Victoria University of Wellington

Hou X, Liu S, Zhu Y, Yang Y (2020). Evaluation of gas contents for a multi-seam deep coalbed methane reservoir and their geological controls: in situ direct method versus indirect method. Fuel, 265: 116917

Jin K, Cheng Y, Wang L, Dong J, Guo P, An F, Jiang L (2015). The effect of sedimentary redbeds on coalbed methane occurrence in the Xutuan and Zhaoji Coal Mines, Huaibei Coalfield, China. Int J Coal Geol, 137: 111–123

Jing G, Chen Z, Hui G (2021). A novel model to determine gas content in naturally fractured shale. Fuel, 306: 121714

Kędzior S, Kotarba M J, Pękała Z (2013). Geology, spatial distribution of methane content and origin of coalbed gases in Upper Carboniferous (Upper Mississippian and Pennsylvanian) strata in the south-eastern part of the Upper Silesian Coal Basin, Poland. Int J Coal Geol, 105: 24–35

Kinnon E C P, Golding S D, Boreham C J, Baublys K A, Esterle J S (2010). Stable isotope and water quality analysis of coal bed methane production waters and gases from the Bowen Basin, Australia. Int J Coal Geol, 82(3−4): 219–231

Kissell F N, McCulloch C M, Elder C H (1973). The direct method of determining methane content of coalbeds for ventilation design. US Department of Interior, Bureau of Mines

Lei H, Dai L, Cao J, Li R, Wang B (2023). Experimental study on rapid determination method of coal seam gas content by indirect method. Processes (Basel), 11(3): 925

Li Q, Pang X, Tang L, Chen G, Shao X, Jia N (2018a). Occurrence features and gas content analysis of marine and continental shales: a comparative study of Longmaxi Formation and Yanchang Formation. J Nat Gas Sci Eng, 56: 504–522

Li S, Tang D, Pan Z, Xu H, Tao S, Liu Y, Ren P (2018b). Geological conditions of deep coalbed methane in the eastern margin of the Ordos Basin, China: implications for coalbed methane development. J Nat Gas Sci Eng, 53: 394–402

Li W, Li X, Zhao S, Li J, Lu S, Liu Y, Huang S, Wang Z, Wang J (2022). Evaluation on carbon isotope fractionation and gas-in-place content based on pressure-holding coring technique. Fuel, 315: 123243

Lin X, Liu C, Wang Z (2023). The influencing factors of gas

adsorption behaviors in shale gas reservoirs. Front Earth Sci (Lausanne), 10: 1021983

Liu S, Harpalani S (2013). Permeability prediction of coalbed methane reservoirs during primary depletion. Int J Coal Geol, 113: 1–10

Luo X, Zhang X, Zhang L, Huang G (2017). Visualization of Chinese CBM research: a scientometrics review. Sustainability (Basel), 9(6): 980

Mavor M J, Owen L B, Pratt T J (1990). Measurement and evaluation of coal sorption isotherm data. ln: SPE Annual Technical Conference and Exhibition 10.2118/20728-MS

Metcalfe R S, Yee D, Seidle J P, Puri R (1991). Review of research efforts in coalbed methane recovery. In: SPE Asia-Pacific Conference

Miao F, Wu D, Liu X, Xiao X, Zhai W, Geng Y (2022). Methane adsorption on shale under in situ conditions: gas-in-place estimation considering *in situ* stress. Fuel, 308: 121991

Ou C, Li C, Zhi D, Xue L, Yang S (2018). Coupling accumulation model with gas-bearing features to evaluate low-rank coalbed methane resource potential in the southern Junggar Basin, China. AAPG Bull, 102(1): 153–174

Qin Y, Moore T A, Shen J, Yang Z, Shen Y, Wang G (2018). Resources and geology of coalbed methane in China: a review. Int Geol Rev, 60(5−6): 777–812

Saghafi A (2017). Discussion on determination of gas content of coal and uncertainties of measurement. Int J Min Sci Technol, 27(5): 741–748

Scott A R (2002). Hydrogeologic factors affecting gas content distribution in coal beds. Int J Coal Geol, 50(1−4): 363–387

Shtepani E, Noll L A, Elrod L W, Jacobs P M (2010). A new regression-based method for accurate measurement of coal and shale gas content. SPE Reservoir Eval Eng, 13(2): 359–364

Smith D M, Williams F L (1984). Direct method of determining the methane content of coal—a modification. Fuel, 63(3): 425–427

Teng J, Yao Y, Liu D, Cai Y (2015). Evaluation of coal texture distributions in the southern Qinshui Basin, north China: investigation by a multiple geophysical logging method. Int J Coal Geol, 140: 9–22

Waechter N B, Hampton G L, Shipps J C (2004). Overview of coal and shale gas measurement: field and laboratory procedures. ln: International Coalbed Methane Symposium: University of Alabama, Tuscaloosa: Alabama

Wang D, Cheng Y, Yuan L, Wang C, Wang L (2023). Implications of geological conditions on gas contents: a case study in the Pingdingshan Coalfield. Energy Fuels, 37(9): 6465–6478

Wang G, Qin Y, Xie Y, Shen J, Wang B, Du L, Guo J (2018a). The spatial distribution of CBM systems under the control of structure and sedimentation: the Gujiao Block as an example. J Geol Soc India, 92(6): 721–731

Wang L, Cheng L B, Cheng Y P, Liu S, Guo P K, Jin K, Jiang H (2015). A new method for accurate and rapid measurement of underground coal seam gas content. J Nat Gas Sci Eng, 26: 1388–1398

Wang Y, Liu D, Cai Y, Yao Y, Zhou Y (2018b). Evaluation of structured coal evolution and distribution by geophysical logging methods in the Gujiao Block, northwest Qinshui Basin, China. J Nat Gas Sci Eng, 51: 210–222

Warwick P D, Breland F C Jr, Hackley P C (2008). Biogenic origin of coalbed gas in the northern Gulf of Mexico Coastal Plain, USA. Int J Coal Geol, 76(1−2): 119–137

Xu H, Pan Z, Hu B, Liu H, Sun G (2020). A new approach to estimating coal gas content for deep core sample. Fuel, 277: 118246

Yang C, Qiu F, Xiao F, Chen S, Fang Y (2023). CBM gas content prediction model based on the ensemble tree algorithm with Bayesian hyper-parameter optimization method: a case study of Zhengzhuang Block, southern Qinshui Basin, north China. Processes (Basel), 11(2): 527

Yang Y, Liu S (2019). Estimation and modeling of pressure-dependent gas diffusion coefficient for coal: a fractal theory-based approach. Fuel, 253: 588–606

Zhao S, Lu S, Wu J, Li W, Liu Y, Li J, Zhang J, Xia Z, Huang S (2023). Comparison and verification of gas-bearing parameter evaluation methods for deep shale based on the pressure coring technique. Energy Fuels, 37(3): 2066–2077

Zhao W, Cheng Y, Pan Z, Wang K, Liu S (2019). Gas diffusion in coal particles: a review of mathematical models and their applications. Fuel, 252: 77–100

Zhu C J, Lin B Q (2015). Effect of igneous intrusions and normal faults on coalbed methane storage and migration in coal seams near the outcrop. Nat Hazards, 77(1): 17–38